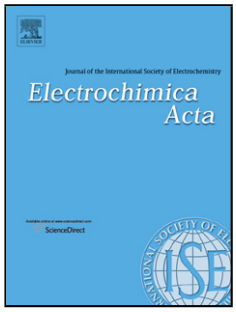


Title: Mesoporous amorphous tungsten oxide electrochromic films: a Raman analysis of their good switching behavior

Author: Dafni Chatzikyriakou Natacha Krins Bernard Gilbert Pierre Colson Jennifer Dewalque Jessica Denayer Rudi Cloots Catherine Henrist

PII: S0013-4686(14)01154-2
DOI: http://dx.doi.org/doi:10.1016/j.electacta.2014.05.139
Reference: EA 22834

To appear in: *Electrochimica Acta*

Received date: 17-12-2013
Revised date: 26-5-2014
Accepted date: 26-5-2014

Please cite this article as: D. Chatzikyriakou, N. Krins, B. Gilbert, P. Colson, J. Dewalque, J. Denayer, R. Cloots, C. Henrist, Mesoporous amorphous tungsten oxide electrochromic films: a Raman analysis of their good switching behavior, *Electrochimica Acta* (2014), http://dx.doi.org/10.1016/j.electacta.2014.05.139

**Title:** Mesoporous amorphous tungsten oxide electrochromic films: a Raman analysis of their good switching behavior

**Authors:** Dafni Chatzikyriakou[a], Natacha Krins[a], Bernard Gilbert[b], Pierre Colson[a], Jennifer Dewalque[a], Jessica Denayer[a], Rudi Cloots[a], Catherine Henrist[a]

[a] Group of Research in Energy and Environment from materials (GreenMat), Department of Chemistry, University of Liege, Allée de la Chimie 3 4000, Liege 1, Belgium

[b] Laboratory of Analytical Chemistry, Department of Chemistry, University of Liege, Allée de la Chimie 3 4000, Liege 1, Belgium

**Contact details of the corresponding author:** Catherine Henrist

E-mail address: Catherine.henrist@ulg.ac.be

University of Liege - Chemistry Department, Group of Research in Energy and Environment from Materials (GREEnMat) Allée de la chimie 3, Building B6 4000 Liege (Belgium)

Phone number: +32 4 366 3438

Fax number: +32 4 366 4747

The intercalation and de-intercalation of lithium cations in electrochromic tungsten oxide thin films are significantly influenced by their structural and surface characteristics.

In this study, we prepared two types of amorphous films via the sol-gel technique: one dense and one mesoporous in order to compare their response upon lithium intercalation and de-intercalation.

According to chronoamperometric measurements, $Li^+$ intercalates/de-intercalates faster in the mesoporous film (24s/6s) than in the dense film (48s/10s). The electrochemical measurements (cyclic voltammetry and chronoamperometry) also showed worse reversibility for the dense film compared to the mesoporous film, giving rise to important $Li^+$ trapping and remaining coloration of the film. Raman analysis showed that the mesoporous film provides more accessible and various W-O surface bonds for $Li^+$ intercalation. On the contrary, in the first electrochemical insertion and de-insertion in the dense film, $Li^+$ selectively reacts with a few surface W-O bonds and preferentially intercalates into pre-existing crystallites to form stable irreversible $Li_xWO_3$ bronze.

## 1. Introduction

Tungsten oxide thin films have been the object of research in numerous recent publications due to their promising properties in gas sensing [1], photocatalysis [2, 3] and electrochromic devices [4-6]. In the latter case, because of their superior coloration efficiency, chemical stability, electronic and ionic conductivity [7], tungsten oxide thin films expanded the horizons from the experimental level to the commercialization in the area of □smart windows''[6].

Tungsten oxide ($WO_3$ or $WO_3.xH_2O$ or $WO_y$) consists of clusters with corner and edge sharing $WO_6$ octahedra, linked together with W-O-W bonds or water bridges [8-10] and presenting lattice channels. Depending on the tilting angles of $WO_6$, the material can adopt monoclinic, triclinic, orthorhombic, tetragonal and cubic crystalline structure ($ReO_3$) [8] or it can be amorphous with the same but randomly oriented building units ($WO_6$) [9].

The electrochromic effect generally involves the simultaneous insertion of electrons (provided by an external potential) and cations (such as lithium or proton cations) and the subsequent formation of coloring centers ($W^{5+}$) [11]. The inserted cations [10] could either reside into the structural channels created by the linkage of $WO_6$ building units or react with the host's bridging oxygens [8,9] by breaking network's W-O-W chains and creating new W=O bonds [12-17] according to the equation:

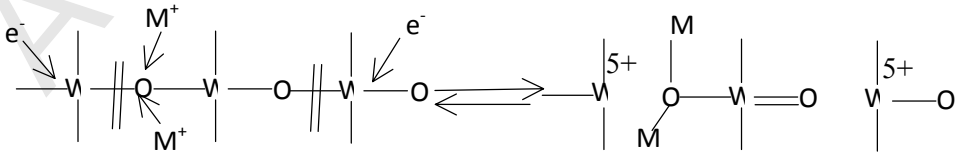


Contrarily, Ohtsuka et al. [18] based on their Raman and infrared findings, claim that coloration originates from the reaction of W=O bonds with the cations ($H^+$) and the subsequent formation of colored $W^{5+}$-OH, but this hypothesis was ruled out in later publications [14]. Others [11, 19]

suggested that cations react with the bridging oxygens at low intercalated charge but at higher amounts they react with W=O as well.

In this study, we highlight the role of film's structure and surface chemistry on the chemical ''pathways'' of lithium cations inside the material. For this purpose, we prepared two types of amorphous films by sol-gel technique: one dense and one mesoporous (with much higher surface to bulk ratio). We investigated their response upon lithium intercalation and de-intercalation by electrochemistry and Raman spectroscopy. Based on this, we show the different intercalation sites existing in the two films. We describe the nature of cations' trapping sites observed in the dense film and explain the superior switching properties of the mesoporous film.

## 2. Experimental

### *2.1 Synthesis of the acetylated peroxotungstic acid precursor (APTA)*

We prepared precursor's powder according to N. Sharma et al. [20]. In detail, a 150mL flask containing 40mL of hydrogen peroxide (29.0-31.0%, Merck) and 4mL of milliQ water was placed in an ice-bath and 6.5g of W powder (particle size 12μm, 99.9%, Aldrich) were added in small lots. The mixture was stirred at low temperature for about 30 min. After the ice-bath was removed, a condenser was placed at the top of the flask and the mixture was allowed to stir overnight at room temperature until all W was dissolved. Then, 40mL of glacial acetic acid were added (Mobi-lab & Labotec) and the solution was heated at 55$^{o}$C for 3h. The yellowish powder (~7g) was recovered by evaporating the solvents in the rotary evaporator at a temperature of 55-60$^{o}$C.

*2.2 Deposition of mesoporous and dense $WO_3$ thin films*

We prepared $WO_3$ thin films following the experimental procedure of W. Wang et al. [21]. Typically, 1g of tungsten precursor APTA was dissolved in 2g of milliQ water and 1g of absolute ethanol (Fischer Scientific). The solution was stirred at room temperature for 2h. The surfactant's solution was prepared by dissolving 0.2g Brij-C10 (Mn~683, Aldrich) in 2.5g of milliQ water and 1.25g of absolute ethanol and the mixture was stirred in a water-bath at 40°C for 2h. After mixing both solutions (APTA and surfactant), the final solution was stirred for 1h at room temperature before using. For the dense films, the same procedure was followed, without the addition of the surfactant. However it was observed that the adherence of the film was seriously reduced without the surfactant and thus a very small amount of Brij-C10 was added.

The $WO_3$ thin films were deposited on pre-cleaned glass substrates ($SnO_2$:F coated glass substrates, TEC15, 3.2x23x19mm, Dyesol) and silicon wafers. The substrates were cleaned by consecutive immersion under sonication in milliQ water (5min), acetone (15 min) and ethanol (15 min). Then, the substrates were dip-coated in the aforementioned final solution at a constant dipping speed (2.5mm/s) and controlled relative humidity (50%). After deposition, the films are left in the chamber for 5 min before being thermally stabilized in an oven at 170°C for 1h in order to evaporate the remaining solvents and initiate the polymerization of the film. Finally the films were calcined at a high temperature under air (heating ramp 1°C/min, natural cooling down in the furnace) to induce the formation of the oxide. The dense films were calcined at 300°C for 1h to avoid crystallization [22]. The mesoporous films were calcined at 350°C for 2h. Indeed, the presence of surfactant in the material was reported to delay the crystallization of tungsten oxide

[23]. Moreover, such a higher temperature for a longer period of time is required to ensure the total elimination of the surfactant.

We prepared thicker dense films for Raman spectroscopy purpose, in order to reach a detectable signal. The deposition process was repeated 3 times with intermediate stabilization at 170°C for 1h, before final calcination.

After calcination, dense films are transparent while mesoporous film possesses a pale yellow-brown color.

*2.3 Characterization techniques*

*2.3.1 Structural and microstructural characterizations*

We performed X-ray diffraction on a Bruker D8 diffractometer (CuKalpha radiation) in grazing incidence configuration with an incident angle of $1^o$, a 2-theta range from $10^o$ to $30^o$, a step size of $0.02^o$ and a scan speed of 1s/step.

TEM micrographs were acquired at an acceleration voltage of 200kV in bright field (BF) and dark field (DF) modes (Tecnai, G2, Twin, FEI). Films were scratched from the substrates, sonicated in ethanol and then deposited on a carbon-coated grid.

Thickness of $WO_3$ films was determined by mechanical profilometry (Dektak 150, VEECO) on FTO/glass substrates. The thickness of dense films was found between 30-50nm and the thickness of mesoporous films was between 60-80nm.

The amount of $WO_3$ in dense and mesoporous films was compared from their X-ray emission spectrum under electron beam in a SEM microscope (FEG- ESEM XL30, 15kV, FEI and EDS spectrometer, Bruker). We recorded the intensity of W Lα peak and compared to a pure W

standard to calculate the so-called k-ratio of tungsten atom in the films. We used this k-ratio value to normalize the quantitative data in electrochemical experiments.

*2.3.2 Cyclic voltammetry and chronoamperometry*

The electrochemical properties were determined using a three electrode configuration (see Figure S.1, Supplementary information) in which the working electrode consisted of the dip-coated $WO_3$ films deposited on FTO/glass substrates in contact with a 0.5M $LiClO_4$ (≥95.0%, Aldrich) in anhydrous propylene carbonate (99.7% , Aldrich) solution. The reference electrode was an Ag/AgCl/KCl (3.5M) and the counter electrode was a platinum foil. The experiments were carried out on an SP-200 BioLogic potensiostat with an EC-Lab express software for collection and analysis of data. Prior to each electrochemical measurement, the electrolyte solution was bubbled for 10 min with purified $N_2$ gas in order to purge dissolved moisture and oxygen. Afterwards the cell was let in an open circuit voltage for 1 min in order to reach equilibrium conditions. Two kinds of electrochemical measurements were conducted, cyclic voltammetry and chronoamperometry. In cyclic voltammetry, current was measured against the applied voltage in the range of ±1V at a constant voltage scan rate. Different scan rates were tested between 3-20mV $s^{-1}$. In chronoamperometric measurements, current was measured with respect to time at constant voltage steps (-1V for 120s, +1V for 120s, 0V for 10s).

*2.3.3 Raman and IR spectra*

Raman measurements were performed directly on films deposited on FTO/glass substrates using a Horiba- Jobin Yvon LabRam 300 spectrometer equipped with a microscope (x100 Olympus objective). The excitation laser was a He-Ne (Melles Griot) emitting at 632.8 nm and the power

at the sample was 0.6 mW. For each sample, the Raman spectrum of the glass was recorded on a film-free area and quantitatively subtracted (until disappearance of the silicate 1100 $cm^{-1}$ band). For the coloration process, the sample was subjected to -1V for 120s and for the bleaching process the film was subjected to -1V for 120s and then at +1V for 120s. Before acquisition, the electrochemically modified films were rinsed with pure acetonitrile in order to remove any propylene carbonate's residues.

IR spectra were recorded in transmission mode from films deposited on silicon wafers using a Bruker Equinox 55 FTIR instrument. The reference was a bare silicon wafer.

## 3. Results and discussion

### *3.1 Structural characterization before the electrochemical insertion of $Li^+$*

Figure 1 presents the TEM micrographs of the two films along with a Fast-Fourier Transform of the image. Dense film possesses a compact and smooth surface (Figure 1.a) after calcination, while mesoporous film consists of regular pores with diameters of about 2-3nm, pore-to-pore distance of about 6nm and wall thickness of about 3-4nm (Figure 1.b).

Figure 1: TEM images of a (a) dense and a (b) mesoporous film. In the inset of b, a Fast-fourier transform image depicting pair of spots, corresponding to periodic structures with different orientations

In this study we investigate amorphous materials rather than crystalline ones in order to preserve the ordered mesoporosity and to emphasize on its role in the electrochemical performance of

tungsten oxide films (see diffractograms in Figure S.2, Supplementary information). Moreover as mentioned in the literature, crystalline materials increase the energy barrier for lithium ions and thus their electrochemical capacity is inferior than their amorphous counterparts [22, 24]. However, dense film possesses a small number of crystallites, not detectable by the X-Ray diffractograms, as inferred by the TEM dark-field micrographs in Figure 2.a (bright patches, 30-40nm). This evidences that crystallization is already initiated in the dense film unlike the mesoporous one which is completely amorphous (Figure 2.b) under the aforementioned experimental conditions. This is in accordance with other publications which report that the existence of surfactant in mesoporous films delays the initiation of crystallization [20].

Figure 2: Dark-field micrographs of a (a) dense film (b) mesoporous film before Li intercalation

FT-IR spectrum (Figure 3) shows that mesoporous films contain a great number of hydroxyls and water molecules physically or chemically absorbed inside the pores of the material [16]. Therefore mesoporous films can be described as a $WO_{3-x-y}OH_x.yH_2O$ material with different hydration and hydroxylation modes [16] in the high and medium wavelength regions (2650-3700 $cm^{-1}$, 1620 and 1420 $cm^{-1}$) while dense film is much less hydrated. Apart from this difference, the FT-IR spectra of the two films look very much alike (see table 1).

Figure 3: FT-IR spectra of a dense and a mesoporous film

Table 1: Peak assignment of the FT-IR spectra for a dense and a mesoporous film

*3.2 Switching performances*

Figure 4.a/b present the cyclic voltammograms of the two films acquired at a scan rate of 20mV $s^{-1}$.

At high scan rates (20mV $s^{-1}$), both films are characterized by a smooth voltammogram as a result of their mainly amorphous nature (Figure 4, Figure S.1) [5, 25] and a well-defined anodic peak. Mesoporous film possesses an extra anodic shoulder (0.8-0.9V), probably stemming from the de-intercalation of lithium cations located at different surface sites [2, 21, 23].

Dense film (Figure 4.a) undergoes a modification of its CV curve during the first 6 cycles [26]. From the 6th cycle, it exhibits good persistence and durability upon lithium insertion and de-insertion, as concluded from the superimposition of the curves at long cycling. This film has been tested up to 1000 cycles (Figure S.3) and it was observed that its activity is not severely altered upon consecutive cycling.

Mesoporous film exhibits partial deterioration with cycling (Figure 4.b), which is attributed to its high active surface and to its hydroxylated/hydrated nature (Figure 3) [16, 27]. In such a highly hydroxylated film, exchange reactions possibly occur between the protons of hydroxyl groups and lithium ions and this phenomenon can accelerate film's degradation [2, 23, 28].

Figure 4: Cyclic voltammograms of a) a dense film and b) a mesoporous film at 20mV.sec$^{-1}$. The current density was normalized according to the W content of the two films .

Figure 5: BF-TEM micrographs of a mesoporous film after subjection to -1V for 120s and then to +1V for 120s (20 cycles). Inset: FTT signal depicting a circle, standing for the existence of periodic structure (single periodicity but random orientation) in the TEM image.

In order to investigate $Li^+$ insertion/de-insertion kinetics, we plotted the intercalated charge at the 10$^{th}$ cycle, against the voltage scan rate. As observed in Figure 6.a, in the case of the dense film when the scan rate increases, the intercalated charge progressively decreases, while in mesoporous film it remains somewhat constant. This is direct evidence that the dense film does not have the time to reach equilibrium conditions as the scan rate increases in contrast to the mesoporous film.

Chronoamperometry (Figure 6.b) confirms the above observation. Mesoporous film reaches its steady-state condition faster than the dense film when a constant potential is applied. This is also quantitatively presented in table 2 (time needed to reach the 90% of film's maximum current density).

Figure 6: a) Plot of the inserted charge (10$^{th}$ cycle) in the dense and the mesoporous film vs. the scan rate in cyclic voltammetry b) chronoamperometric measurement (current density vs. time) at the tenth cycle (-1V for 120s and then +1V for 120s). The charge and current density were normalized according to the W content of the films.

After the electrochemical intercalation and de-intercalation of $Li^+$ cations, the films should ideally return to their initial transparency. However the dense film retains its blue color after the measurement. This is due to the incomplete de-intercalation of inserted $Li^+$ in the first cycles, as already detected in the cyclic voltammogram (Figure 4.a). Around 50% of the lithium ions are trapped during the first cycle, as confirmed by the reversibility experiments (Table 2 and Figure 7).

Figure 7: Plots of the fraction of trapped $Li^+$ cations (calculated by the chronoamperometric measurements) vs. the number of cycles for the a) dense and b) mesoporous film

Table 2: Intercalation/de-intercalation times, charge inserted/de-inserted and reversibility values for the dense and mesoporous film.

3.3 Ex-situ Raman analysis

In order to specify the origin of the traps evidenced for the dense film and to better understand where $Li^+$ cations reside inside the material, we performed Raman measurements.

Raman spectra show that before $Li^+$ intercalation the two films exhibit mainly two wide peaks in the high wavelength region. A broad and multicomponent peak (500-850 $cm^{-1}$) is attributed to the stretching vibrations of W-O (bridging/terminal W-OH) and a single band (around 950 $cm^{-1}$) is attributed to W=O bonds [11, 29-31].

Figure 8: Raman spectra of a dense film before (no $Li^+$), after $Li^+$ intercalation and $Li^+$ de-intercalation

The broadness of the peaks and the presence of W=O bonds (which are absent in crystalline materials [11, 13, 30] designate the mainly amorphous nature of the two films. Interestingly, no signature of crystalline structure appears in the Raman spectrum of the dense film (narrow peaks expected at 720 and 810 $cm^{-1}$[31]) in contrast to the TEM dark-field image in Figure 2.a. This probably stems from the low range of ordering and the small number of crystallites in the film.

The network linkage looks somewhat different in the two films: the ratio of various W-O bands in the range 500-850 $cm^{-1}$ is different and the mesoporous film exhibits an extra peak at 558 $cm^{-1}$. Overall, the different W-O peaks appear more distinctly in the mesoporous film in respect to the dense, which we attribute to the high surface to bulk ratio. Those W-O bonds should therefore be preferentially located at the surface of the material.

The peak at 780 $cm^{-1}$ is attributed to the antisymmetric stetching vibration of W-O-W bonds [32]. Different clusters ($W_2O_6$ and $W_3O_8$ according to [33] presumably exist on the surface of the films and their stretching mode of terminal W-O bonds give rise to the peak at 697/692 $cm^{-1}$. The band at 639 $cm^{-1}$ is attributed to the lattice phonon vibrations of $WO_3(H_2O)_x$ [34]. This band is stronger in mesoporous film (633 $cm^{-1}$), confirming its higher degree of hydration. No information was found in the literature regarding the peak at 558 $cm^{-1}$ in the spectrum of the mesoporous film. We presume that this peak originates from longer W-O bonds (curved surface in the pores) associated with water molecules [9].

In the low wavelength region (100-500 $cm^{-1}$) dense film (and to a lesser extend mesoporous film) possesses a broad peak centered at around 300 $cm^{-1}$ related to $W^{4+}$-O bonds and a small band

located at 440 $cm^{-1}$ assigned to the $W^{5+}$=O vibration. This implies that dense film is defined by $WO_{3-x}$ formula and thus it contains W atoms at different valence states ($W^{4+}$,$W^{5+}$,$W^{6+}$) [11, 30, 31, 35].

Figure 9: Raman spectra of a mesoporous film before (no $Li^+$), after $Li^+$ intercalation and $Li^+$ de-intercalation

Upon $Li^+$ intercalation (Figure 8, 9), in the low wavelength region, $Li^+$ cations induce the appearance of distinct peaks (171/164 and 287/278 $cm^{-1}$) in both films, attributed to the stretching (v) and bending vibrations (δ) of O-W-O bonds in $M_xWO_3$ materials [10, 11].

However, a different intercalation behavior of Li cations between the two films appears in the high wavelength region (500-850 $cm^{-1}$).

In the mesoporous film, $Li^+$ cations highly disrupt the W-O lattice bonds located at the surface of the pores, as evidenced by the overall diminution of the broad band in the 500-850 $cm^{-1}$ region.

In the dense film, the peaks at 782 $cm^{-1}$ ( antisymmetric stretching vibration of W-O-W) and 639 $cm^{-1}$ (lattice vibrations of the hydrated oxide $WO_3$. $xH_2O$) slightly shift to lower wavelengths (772/617 $cm^{-1}$) but they remain intact upon lithium intercalation. Contrarily, the peak at 697 $cm^{-1}$, previously assigned to the terminal oxygens of surface clusters, vanishes after lithium intercalation.

These observations suggest that the cations react with the accessible bonds and clusters on the plane surface of dense film, while the porous surface of mesoporous film provides more paths for lithium intercalation, in accordance with the faster kinetics discussed in the previous paragraph.

Interestingly, W=O bands in our systems do not disappear upon $Li^+$ intercalation as stated by others [11, 19]. They only slightly shift to lower wavelengths in both cases (dense film from 947 to 939 $cm^{-1}$ and mesoporous film from 952 to 938 $cm^{-1}$) probably due to the presence of the cations which weaken the strength of the double bond. This displacement, is reversible in both films after lithium extraction.

It is worth noting that no peaks attributed to Li-O bonds appear in the spectra of the two films as already inferred in the literature [11], even though it is already proposed that the cations affect network's vibrations [10-12, 16] instead of residing only within the lattice channels. Bueno et al. [11] support that, at high amounts of lithium insertion, there is a very weak interaction ($W^{5+}$-O ← $Li^+$) between the lithium ions and the network, which immobilizes the ions inside the film (although Li-O bond is not detectable by Raman). Our observation of disappearance of the network's vibrations upon lithium intercalation, corroborates with this suggestion.

Nevertheless, de-insertion of the $Li^+$ cations should revert the films to their initial state.

In the case of the mesoporous film (Figure 9) the spectrum after one complete cycle looks very much alike to the one before the electrochemical insertion, in accordance with the recovered transparency and reversibility values in table 2.

In the dense film, de-intercalation is not homogeneous and two regions co-exist with different structural characteristics (Figure 8). The spectrum acquired in the region 1 looks alike the initial one, before any lithium intercalation. However, in the low wavelength region (200-400$cm^{-1}$) the

broad peak around 300cm$^{-1}$ re-appears with higher intensity, indicating that some reduced tungsten atoms remain. This is in accordance with previous observations and the permanent coloration of the film after the measurement.

In the region 2, a new phase is detected (Figure 8). This spectrum resembles to a great extent with the ones reported for lithiated tungsten oxide films at the initial steps of crystallization [11, 36]. From these references, such a spectrum derives from $Li_xWO_3$ crystallites (see also dark-field TEM micrograph S4). Evidently, a fraction of cations (in accordance with our chronoamperometric results in Figure 7) remains inside the material and resides in the lattice channels of the $WO_6$ octahedra within the pre-existing crystallites. Therefore, we believe that the permanent coloration of the dense film stems from the stable $Li_xWO_3$ crystallites which are formed upon $Li^+$ intercalation.

Finally, the detection of crystallites by Raman after $Li^+$ insertion, suggests that $Li^+$ cations might increase the range of order of the pre-existing crystallites, but further investigations should be carried out in order to verify this assumption.

## 4. Conclusions

In this study, mesoporous and dense films of $WO_3$ were prepared by sol-gel and a comparison between the two has been made in respect to their structural differences and their electrochemical performance upon $Li^+$ intercalation and de-intercalation.

Electrochemical measurements revealed that the mesoporous film possesses faster kinetics and better reversibility towards $Li^+$ intercalation and de-intercalation compared to the dense film. As appeared from Raman spectra, this is probably due to the easily accessible W-O surface bonds in the pores, giving numerous and reversible insertion pathways. However, the high content of hydroxyl groups associated to the high surface-to-volume ratio of mesoporous films facilitates the progressive H-Li exchange upon cycling. This has no consequence on the porous architecture of the film.

In the dense film, $Li^+$ cations selectively react with some terminal W-O bonds leaving unaffected inaccessible W-O bonds. Furthermore a fraction of the intercalated cations reside inside pre-existing crystallites, creating stable $Li_xWO_3$ bronzes. The latter cations remain inside the film even after the completion of the electrochemical reaction. Therefore we believe that these crystallites serve as trapping sites for $Li^+$ cations in the dense film during the first several cycles.

**Acknowledgements:** This work was financed by the Greek A.S. Onassis Public Benefit Foundation (2011-2012) and the Belgian WBI (Wallonie-Brussels International) Scholarship Service (2012-). The authors would also like to thank the SPW (Service Public de Wallonie) for providing through the SMARTSPRAY project (Greenomat call) some of the chemicals and materials needed for the electrochemical measurements. Special acknowledgments to Mr. Gilles Spronck for his technical support and to Professor Benoit Heinrichs for giving access to the profilometry measurements. Finally the authors are grateful to Sebastien Caes for the fruitful discussions and to Cedric Malherbe for his assistance in the acquisition of Raman spectra.

References:

[1] J. Shieh, H.M. Feng, M.H. Hon, H.Y. Juang, WO3 and W-Ti-O thin-film gas sensors prepared by sol-gel dip-coating, Sensors and Actuators, B: Chemical, B86 (2002) 75-80.

[2] S.-H. Baeck, K.-S. Choi, T.F. Jaramillo, G.D. Stucky, E.W. McFarland, Enhancement of photocatalytic and electrochromic properties of electrochemically fabricated mesoporous WO3 thin films, Advanced Materials (Weinheim, Germany), 15 (2003) 1269-1273.

[3] B. Yang, Y. Zhang, E. Drabarek, P.R.F. Barnes, V. Luca, Enhanced Photoelectrochemical Activity of Sol-Gel Tungsten Trioxide Films through Textural Control, Chemistry of Materials, 19 (2007) 5664-5672.

[4] J. Livage, D. Ganguli, Sol-gel electrochromic coatings and devices: A review, Solar Energy Materials & Solar Cells, 68 (2001) 365-381.

[5] C.G. Granqvist, Handbook of Inorganic Electrochromic Materials, Elsevier Science, 1995.

[6] R. Baetens, B.P. Jelle, A. Gustavsen, Properties, requirements and possibilities of smart windows for dynamic daylight and solar energy control in buildings: A state-of-the-art review, Solar Energy Materials and Solar Cells, 94 (2010) 87-105.

[7] A.K. Srivastava, M. Deepa, S. Singh, R. Kishore, S.A. Agnihotry, Microstructural and electrochromic characteristics of electrodeposited and annealed $WO_3$ films, Solid State Ionics, 176 (2005) 1161-1168.

[8] H. Zheng, J.Z. Ou, M.S. Strano, R.B. Kaner, A. Mitchell, K. Kalantar-zadeh, Nanostructured Tungsten Oxide – Properties, Synthesis, and Applications, Advanced Functional Materials, 21 (2011) 2175-2196.

[9] J.V. Gabrusenoks, P.D. Cikmach, A.R. Lusis, J.J. Kleperis, G.M. Ramans, Electrochromic colour centres in amorphous tungsten trioxide thin films, Solid State Ionics, 14 (1984) 25-30.

[10] O. Pyper, A. Kaschner, C. Thomsen, In situ Raman spectroscopy of the electrochemical reduction of $WO_3$ thin films in various electrolytes, Solar Energy Materials and Solar Cells, 71 (2002) 511-522.

[11] P.R. Bueno, F.M. Pontes, E.R. Leite, L.O.S. Bulhões, P.S. Pizani, P.N. Lisboa-Filho, W.H. Schreiner, Structural analysis of pure and LiCF3SO3-doped amorphous WO3 electrochromic films and discussion on coloration kinetics, Journal of Applied Physics, 96 (2004) 2102-2109.

[12] B. Orel, U.O. Krasovec, N. Groselj, M. Kosec, G. Drazic, R. Reisfeld, Gasochromic behavior of sol-gel derived Pd doped peroxopolytungstic acid (W-PTA) nano-composite films, J. Sol-Gel Sci. Technol., 14 (1999) 291-308.

[13] P. Delichere, P. Falaras, M. Froment, A. Hugot-Le Goff, B. Agius, Electrochromism in anodic WO3 films I: Preparation and physicochemical properties of films in the virgin and coloured states, Thin Solid Films, 161 (1988) 35-46.

[14] J.L. Paul, J.C. Lassègues, Infrared Spectroscopic Study of Sputtered Tungsten Oxide Films, Journal of Solid State Chemistry, 106 (1993) 357-371.

[15] B. Orel, N. Grošelj, U.O. Krašovec, R. Ješe, A. Georg, IR Spectroscopic Investigations of Gasochromic and Electrochromic Sol-Gel—Derived Peroxotungstic Acid/Ormosil Composite and Crystalline WO3 Films, Journal of Sol-Gel Science and Technology, 24 (2002) 5-22.

[16] G. Leftheriotis, S. Papaefthimiou, P. Yianoulis, The effect of water on the electrochromic properties of $WO_3$ films prepared by vacuum and chemical methods, Solar Energy Materials & Solar Cells, 83 (2004) 115-124.

[17] J.G. Zhang, D.K. Benson, C.E. Tracy, S.K. Deb, A.W. Czanderna, C. Bechinger, Chromic Mechanism in Amorphous □$WO_3$ Films, Journal of the Electrochemical Society, 144 (1997) 2022-2026.

[18] T. Ohtsuka, N. Goto, N. Sato, Change of the anodic oxide films of tungsten during the electrochromic reaction, Journal of Electroanalytical Chemistry and Interfacial Electrochemistry, 287 (1990) 249-264.

[19] S.-H. Lee, H.M. Cheong, C. Edwin Tracy, A. Mascarenhas, R. Pitts, G. Jorgensen, S.K. Deb, Influence of microstructure on the chemical diffusion of lithium ions in amorphous lithiated tungsten oxide films, Electrochimica Acta, 46 (2001) 3415-3419.

[20] N. Sharma, M. Deepa, P. Varshney, S.A. Agnihotry, FT-IR and absorption edge studies on tungsten oxide based precursor materials synthesized by sol–gel technique, Journal of Non-Crystalline Solids, 306 (2002) 129-137.

[21] W. Wang, Y. Pang, S.N.B. Hodgson, Preparation, characterisation and electrochromic property of mesostructured tungsten oxide films via a surfactant templated sol–gel process from tungstic acid, Journal of Sol-Gel Science and Technology, 54 (2010) 19-28.

[22] J.-H. Choy, Y.-I. Kim, J.-B. Yoon, S.-H. Choy, Temperature-dependent structural evolution and electrochromic properties of peroxopolytungstic acid, J. Mater. Chem., 11 (2001) 1506-1513.

[23] W. Cheng, E. Baudrin, B. Dunn, J.I. Zink, Synthesis and electrochromic properties of mesoporous tungsten oxide, Journal of Materials Chemistry, 11 (2001) 92-97.

[24] S. Sallard, T. Brezesinski, B.M. Smarsly, Electrochromic Stability of WO3 Thin Films with Nanometer-Scale Periodicity and Varying Degrees of Crystallinity, The Journal of Physical Chemistry C, 111 (2007) 7200-7206.

[25] M. Deepa, T.K. Saxena, D.P. Singh, K.N. Sood, S.A. Agnihotry, Spin coated versus dip coated electrochromic tungsten oxide films: Structure, morphology, optical and electrochemical properties, Electrochim. Acta, 51 (2006) 1974-1989.

[26] J. Nagai, T. Kamimori, M. Mizuhashi, Electrochromism in amorphous lithium tungsten oxide films, Solar Energy Materials, 13 (1986) 279-295.

[27] J.G. Zhang, C.E. Tracy, D.K. Benson, S.K. Deb, The influence of microstructure on the electrochromic properties of lithium tungsten oxide ($Li_xWO_3$) thin films. Part I. Ion diffusion and electrochromic properties, J. Mater. Res., 8 (1993) 2649-2656.

[28] T.J. Vink, E.P. Boonekamp, R.G.F.A. Verbeek, Y. Tamminga, Lithium trapping at excess oxygen in sputter-deposited a-WO3 films, J. Appl. Phys., 85 (1999) 1540-1544.

[29] S.-H. Lee, H.M. Cheong, C.E. Tracy, A. Mascarenhas, J.R. Pitts, G. Jorgensen, S.K. Deb, Alternating current impedance and Raman spectroscopic study on electrochromic a-$WO_3$ films, Applied Physics Letters, 76 (2000) 3908-3910.

[30] A. Baserga, V. Russo, F. Di Fonzo, A. Bailini, D. Cattaneo, C.S. Casari, A. Li Bassi, C.E. Bottani, Nanostructured tungsten oxide with controlled properties: Synthesis and Raman characterization, Thin Solid Films, 515 (2007) 6465-6469.

[31] S.-H. Lee, H.M. Cheong, C.E. Tracy, A. Mascarenhas, D.K. Benson, S.K. Deb, Raman spectroscopic studies of electrochromic a-$WO_3$, Electrochimica Acta, 44 (1999) 3111-3115.

[32] B.M. Weckhuysen, J.-M. Jehng, I.E. Wachs, In Situ Raman Spectroscopy of Supported Transition Metal Oxide Catalysts: $^{18}O_2$–$^{16}O_2$ Isotopic Labeling Studies, The Journal of Physical Chemistry B, 104 (2000) 7382-7387.

[33] W. Weltner Jr, D. McLeod Jr, Spectroscopy of tungsten oxide molecules in neon and argon matrices at 4° and 20°K, Journal of Molecular Spectroscopy, 17 (1965) 276-299.

[34] M.F. Daniel, B. Desbat, J.C. Lassegues, B. Gerand, M. Figlarz, Infrared and Raman study of WO3 tungsten trioxides and $WO_3.xH_2O$ tungsten trioxide hydrates, Journal of Solid State Chemistry, 67 (1987) 235-247.

[35] S.-H. Lee, H.M. Cheong, C.E. Tracy, A. Mascarenhas, A.W. Czanderna, S.K. Deb, Electrochromic coloration efficiency of a-$WO_{3-y}$ thin films as a function of oxygen deficiency, Applied Physics Letters, 75 (1999) 1541-1543.

[36] M. Deepa, A.G. Joshi, A.K. Srivastava, S.M. Shivaprasad, S.A. Agnihotry, Electrochromic Nanostructured Tungsten Oxide Films by Sol-gel: Structure and Intercalation Properties, Journal of the Electrochemical Society, 153 (2006) C365-C376.

Highlights

1) Mesoporous films exhibit better electrochemical kinetics compared to the dense films

2) Mesoporous films exhibit better reversibility compared to the dense films

3) $Li^+$cations disrupt $WO_3$ network in a reversible way in the mesoporous film

4) $Li^+$ irreversibly intercalate in the voids of crystallites in the dense film

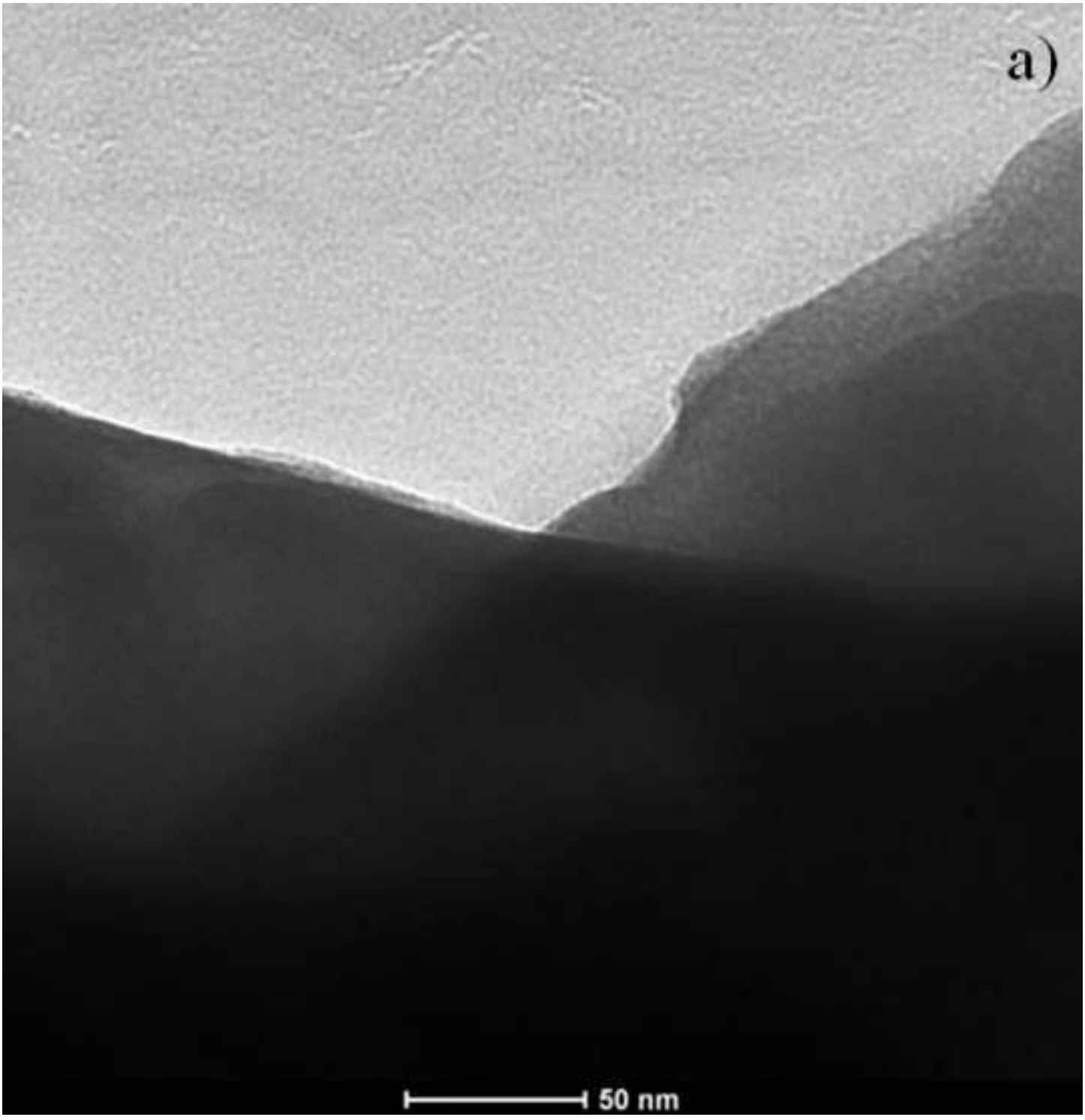

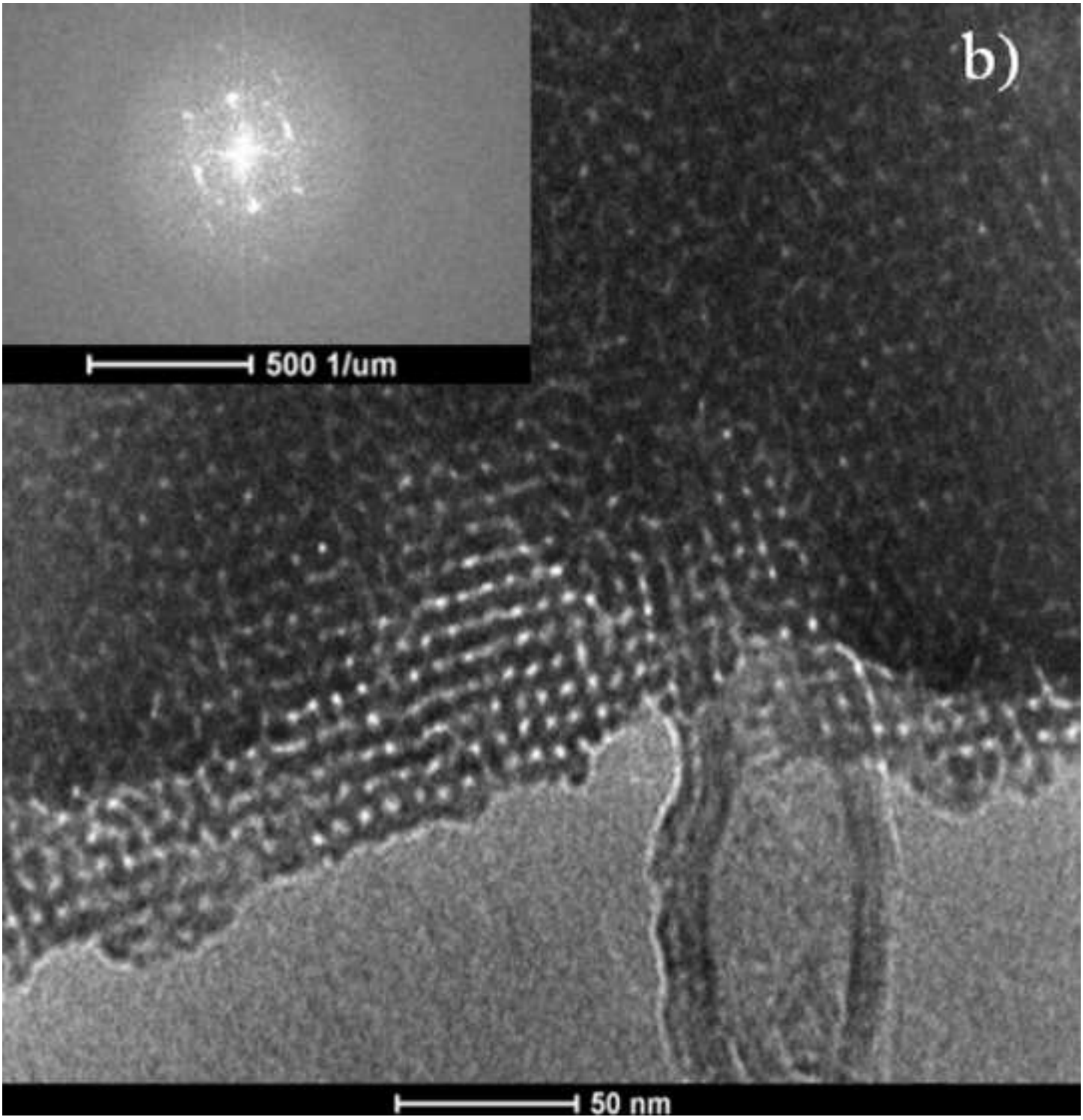

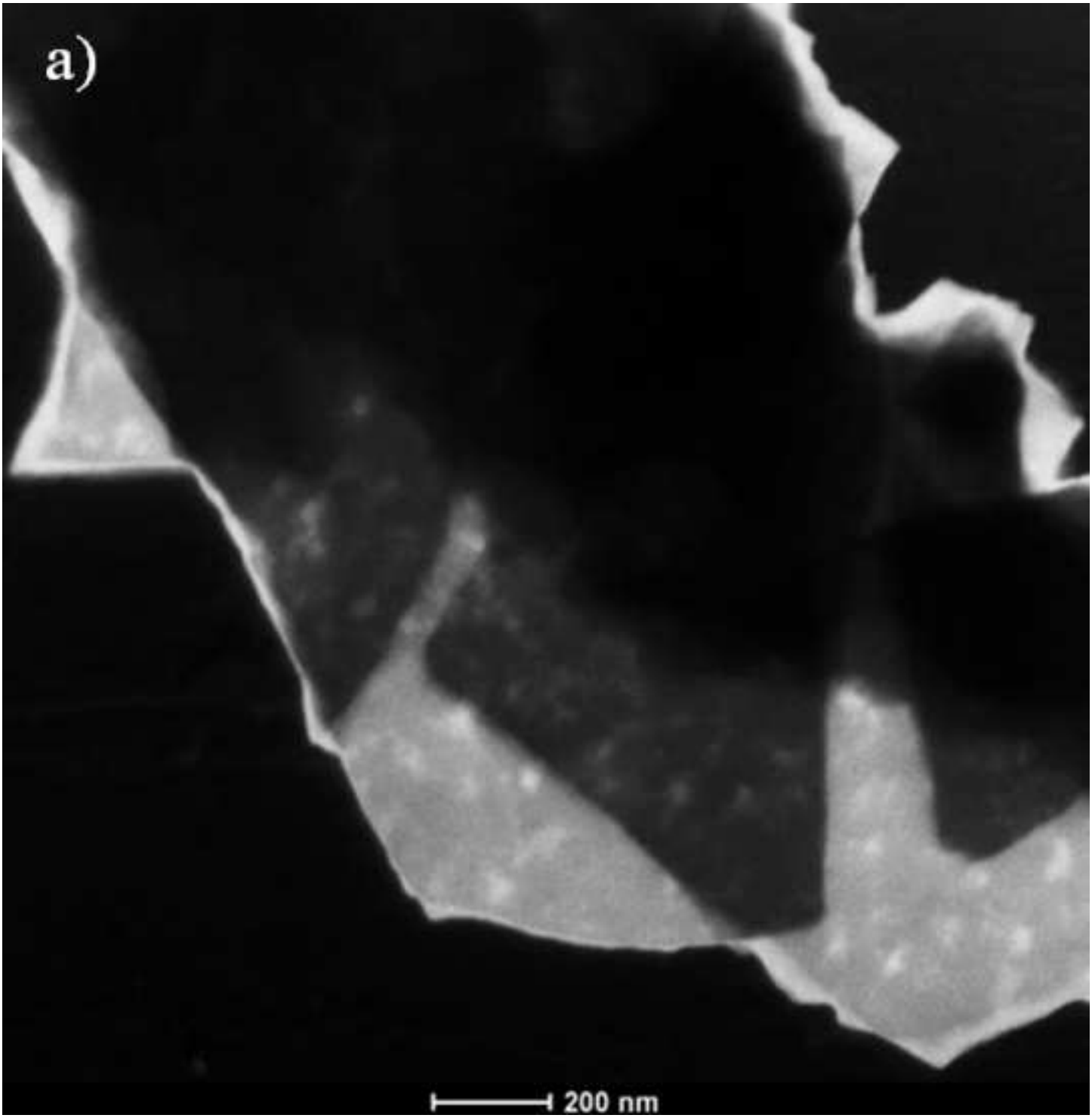

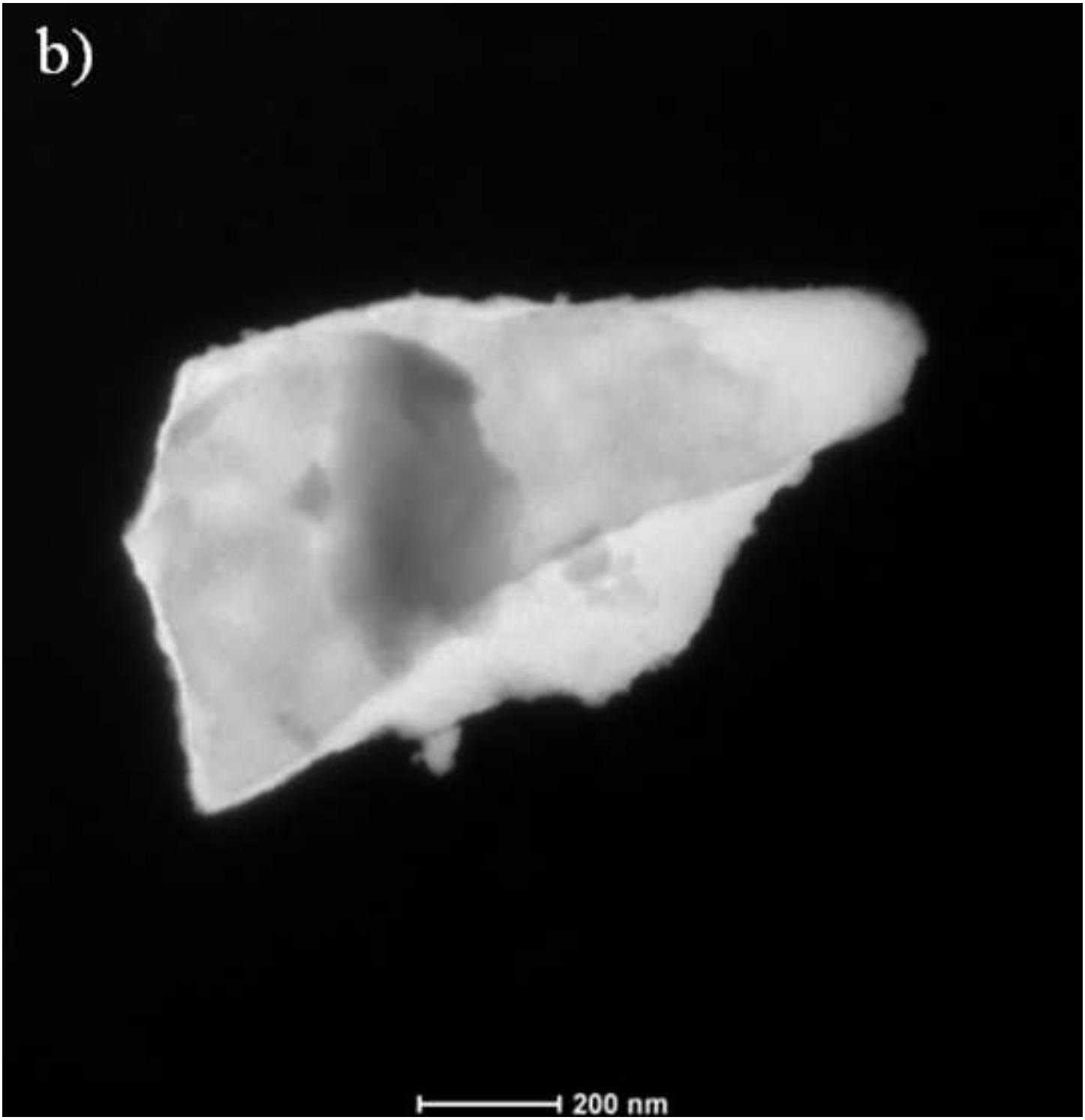

**Figure(s)**

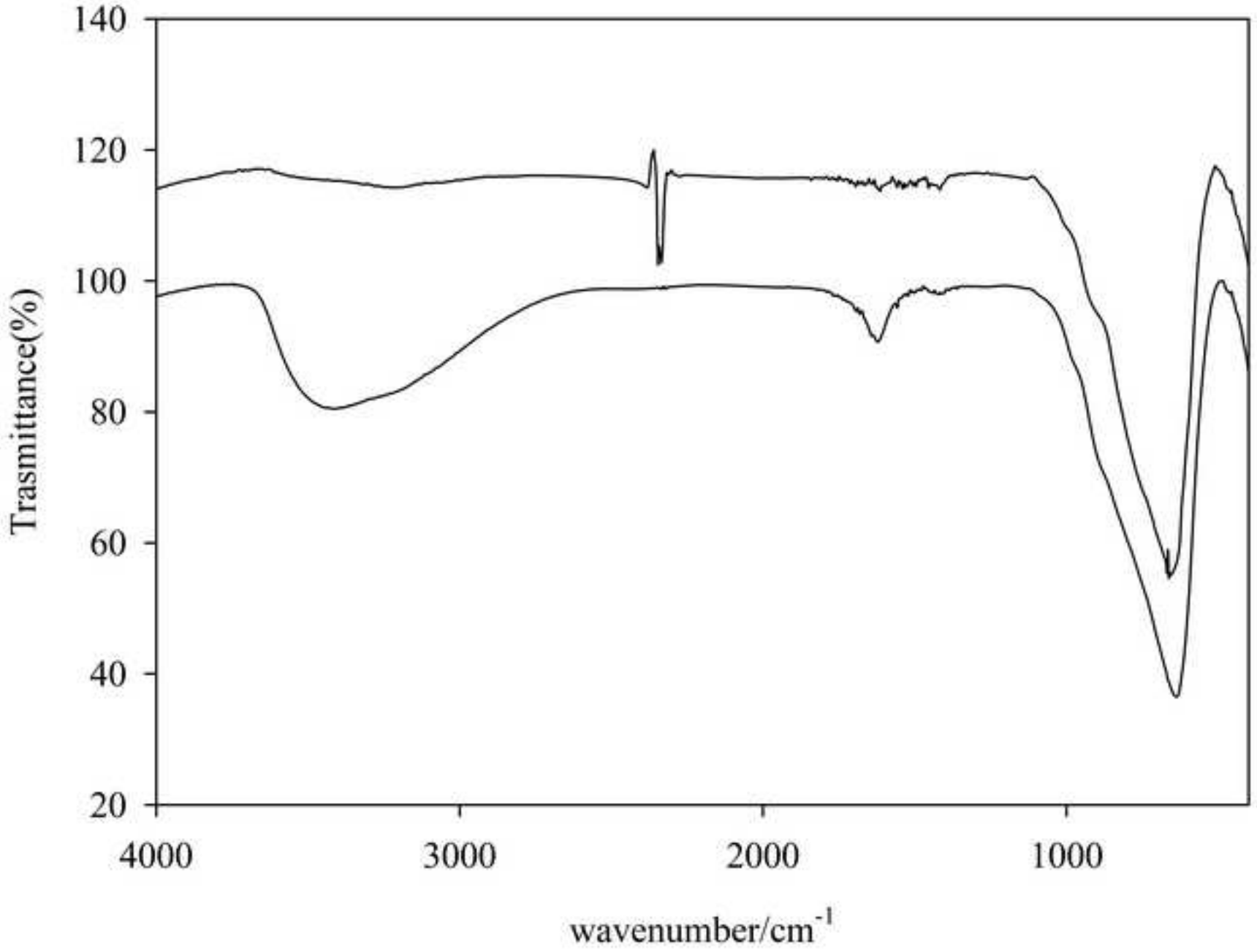
140
120
100
80
60
40
20
Trasmittance(%)
4000
3000
2000
1000
wavenumber/cm-1

**Figure(s)**

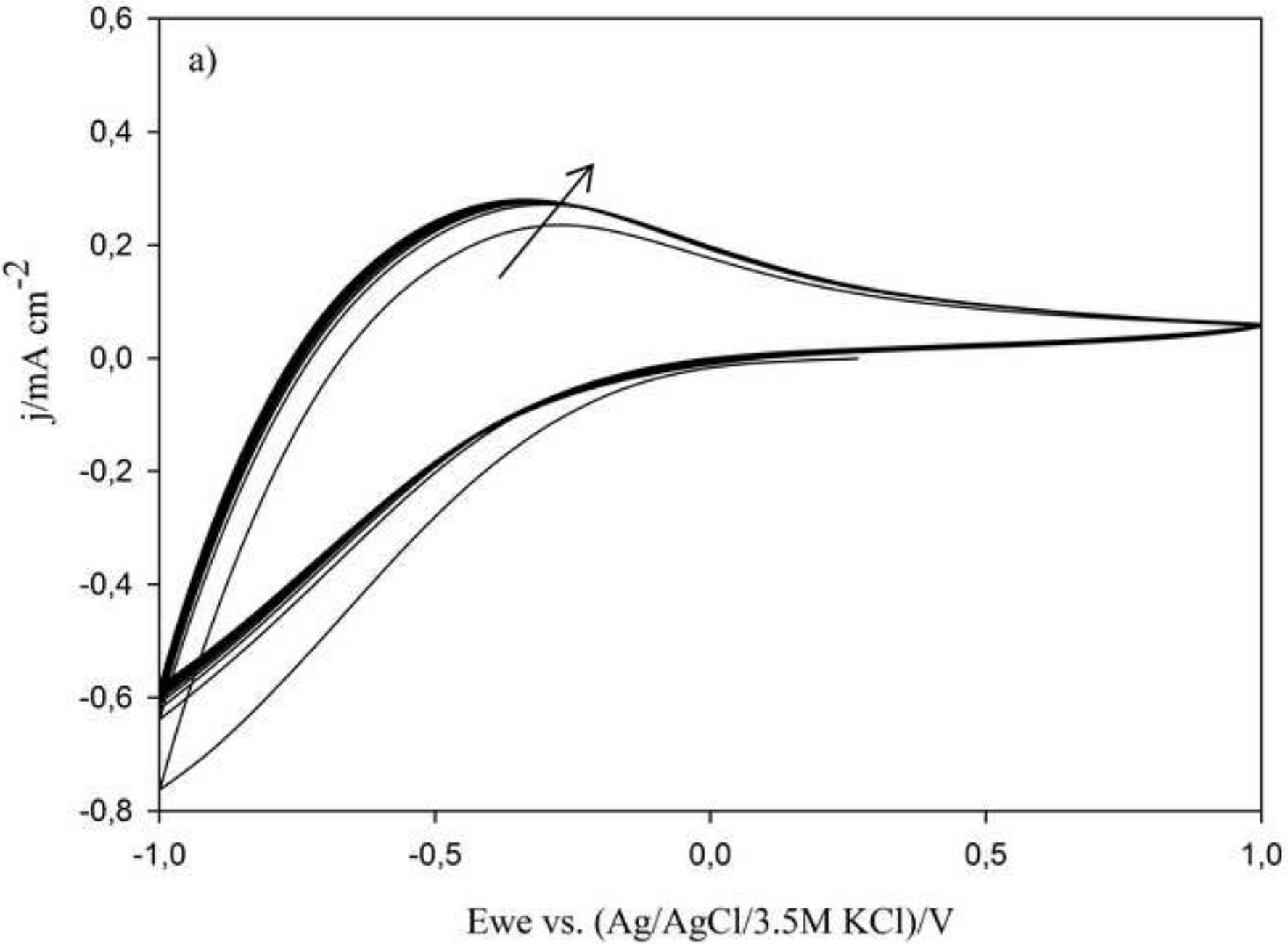
a)
0,6
0,4
0,2
0,0
-0,2
-0,4
-0,6
-0,8
j/mA cm-2
-1,0
-0,5
0,0
0,5
1,0
Ewe vs. (Ag/AgCl/3.5M KCl)/V

**Figure(s)**

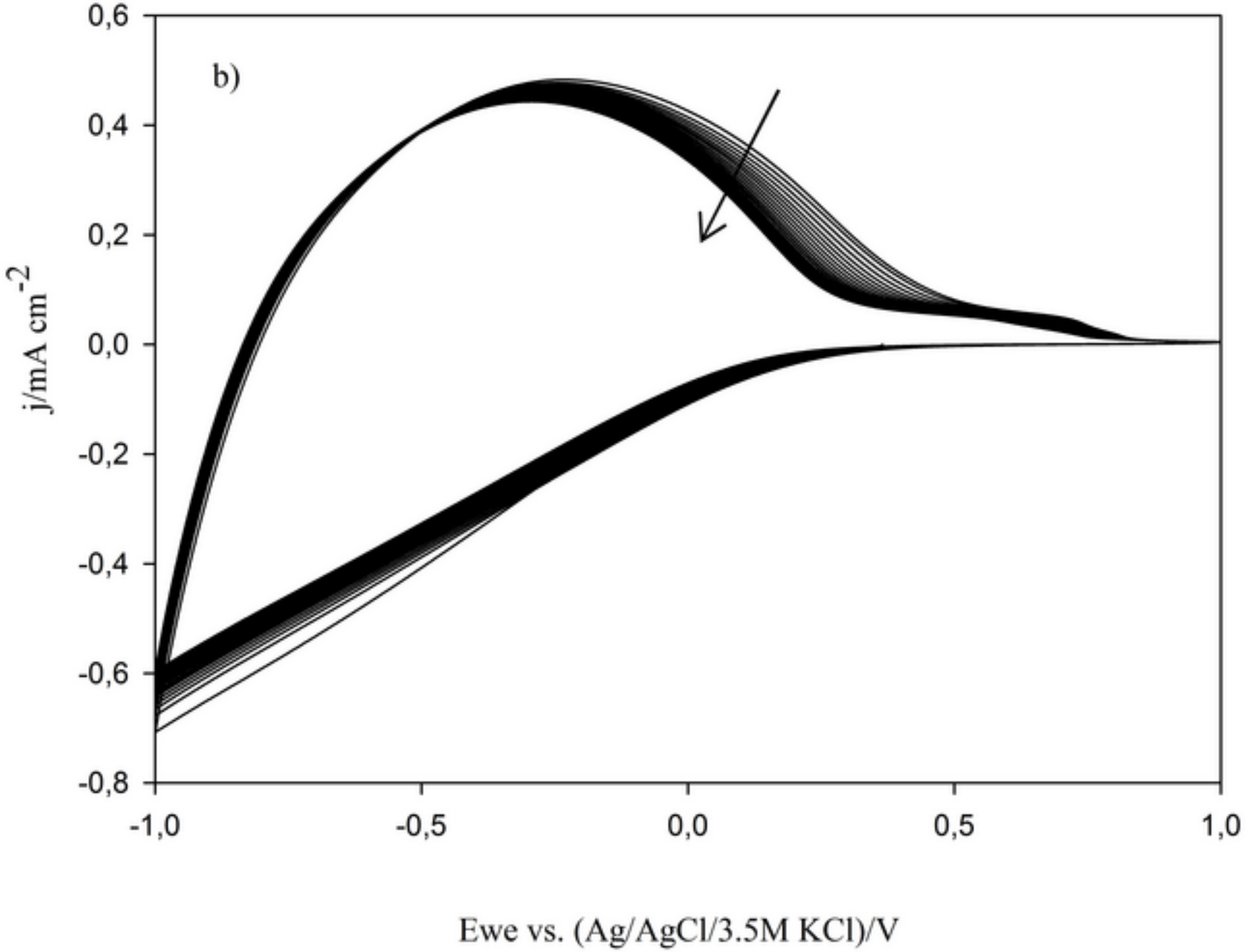
b)
0,6
0,4
0,2
0,0
-0,2
-0,4
-0,6
-0,8
j/mA cm-2
-1,0
-0,5
0,0
0,5
1,0
Ewe vs. (Ag/AgCl/3.5M KCl)/V

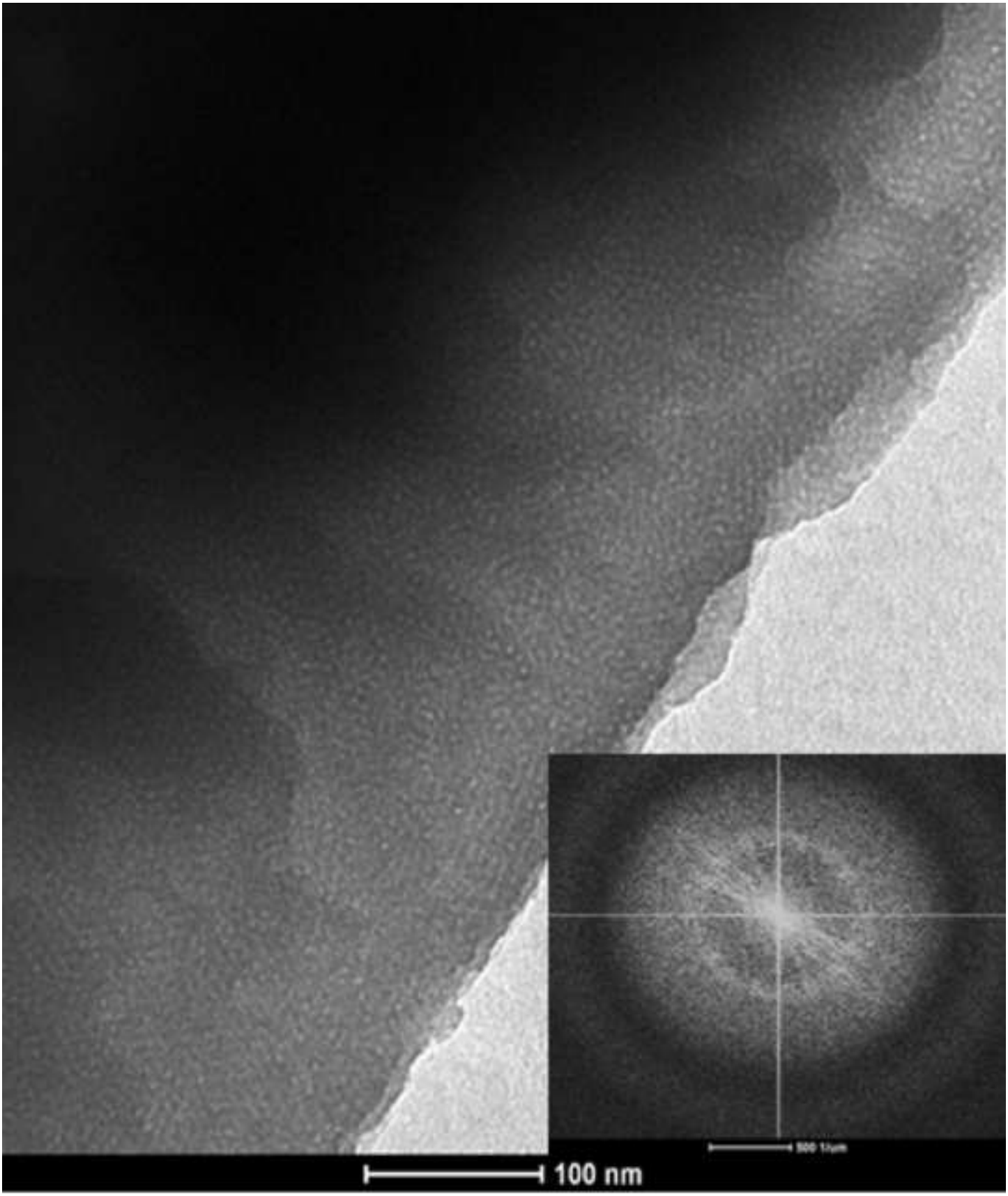

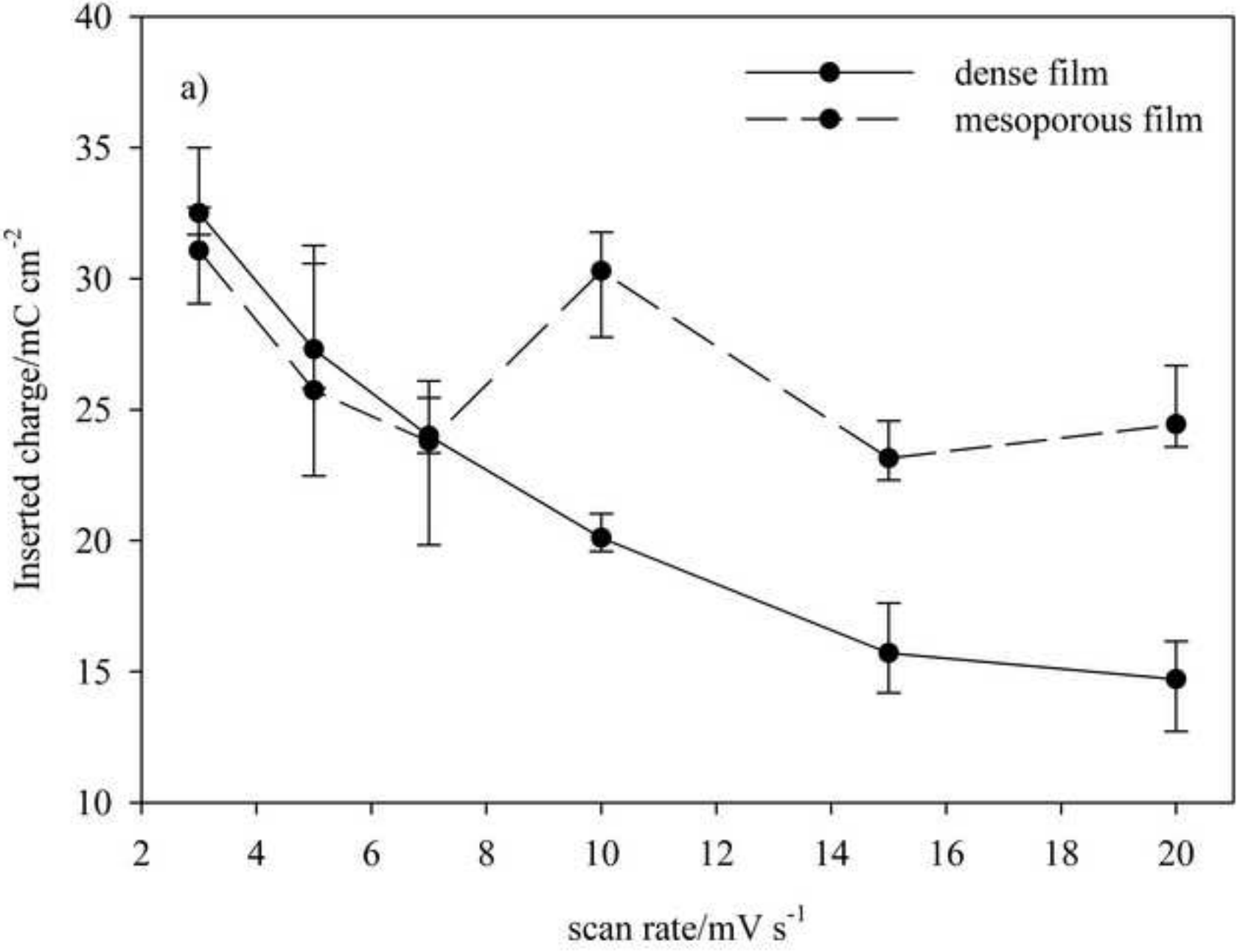
a)
dense film
mesoporous film
Inserted charge/mC cm-2
scan rate/mV s-1
40
35
30
25
20
15
10
2
4
6
8
10
12
14
16
18
20

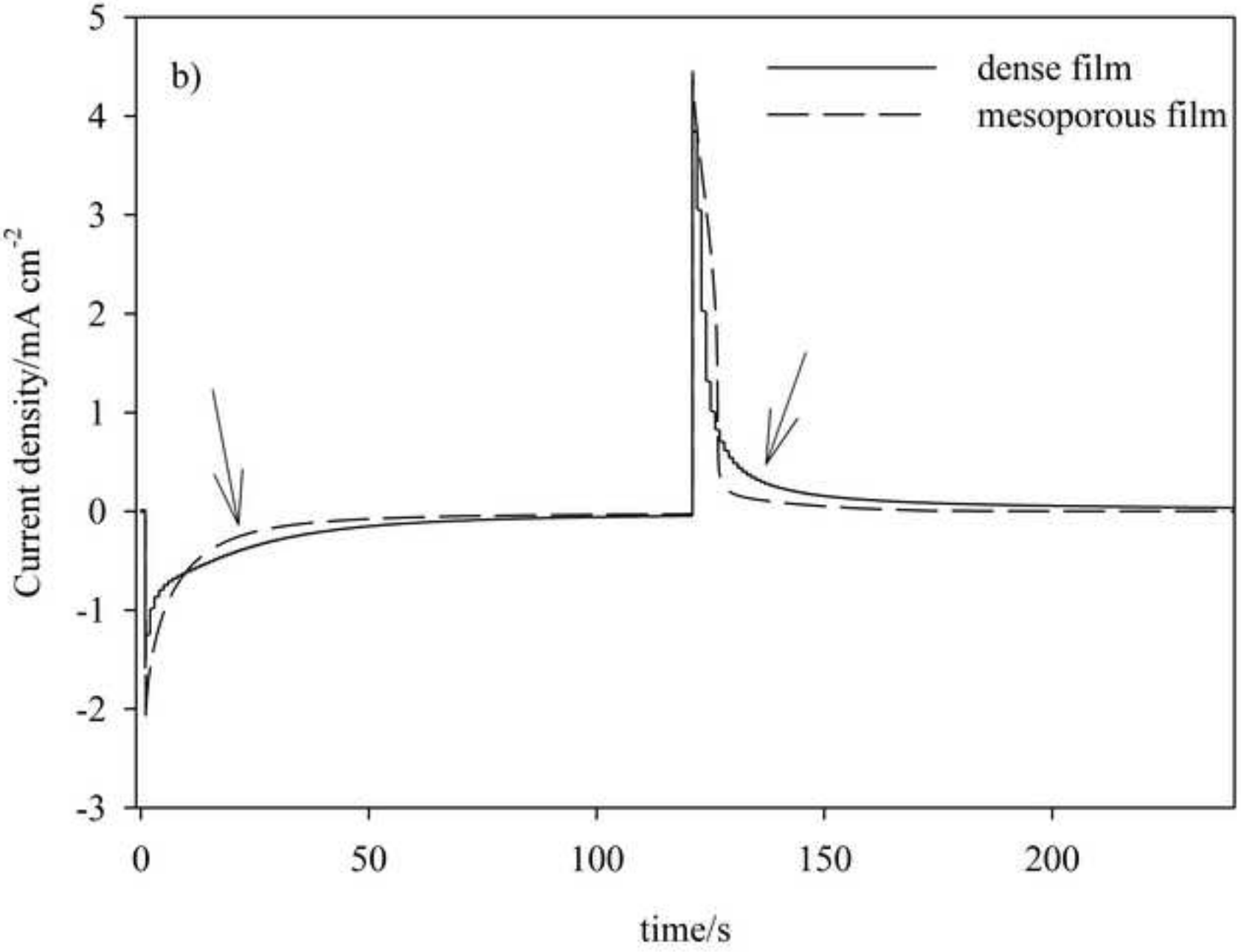
b)
dense film
mesoporous film
Current density/mA cm-2
time/s
5
4
3
2
1
0
-1
-2
-3
0
50
100
150
200

**Figure(s)**

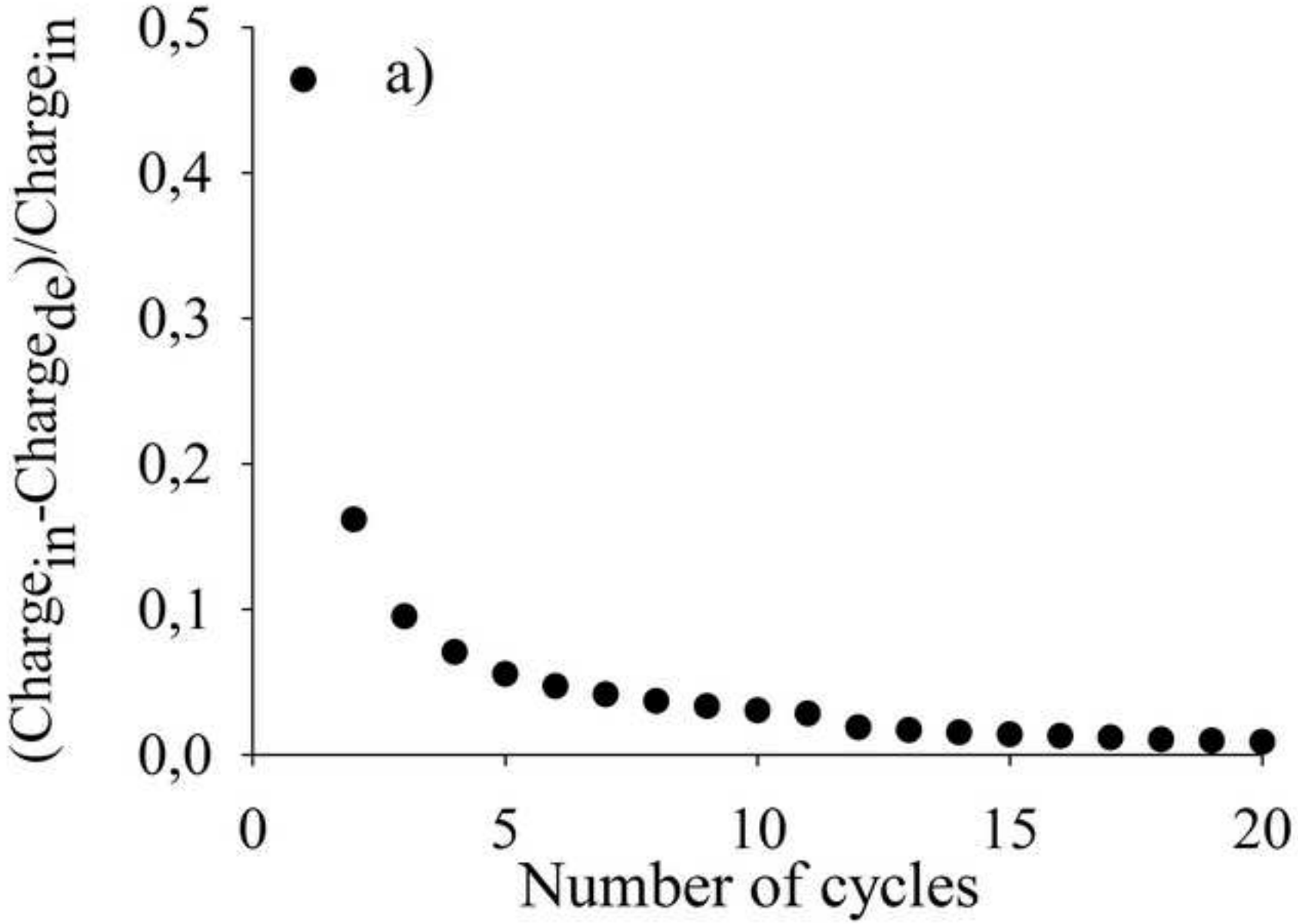
a)
(Charge$_{in}$-Charge$_{de}$)/Charge$_{in}$
0,5
0,4
0,3
0,2
0,1
0,0
0
5
10
15
20
Number of cycles

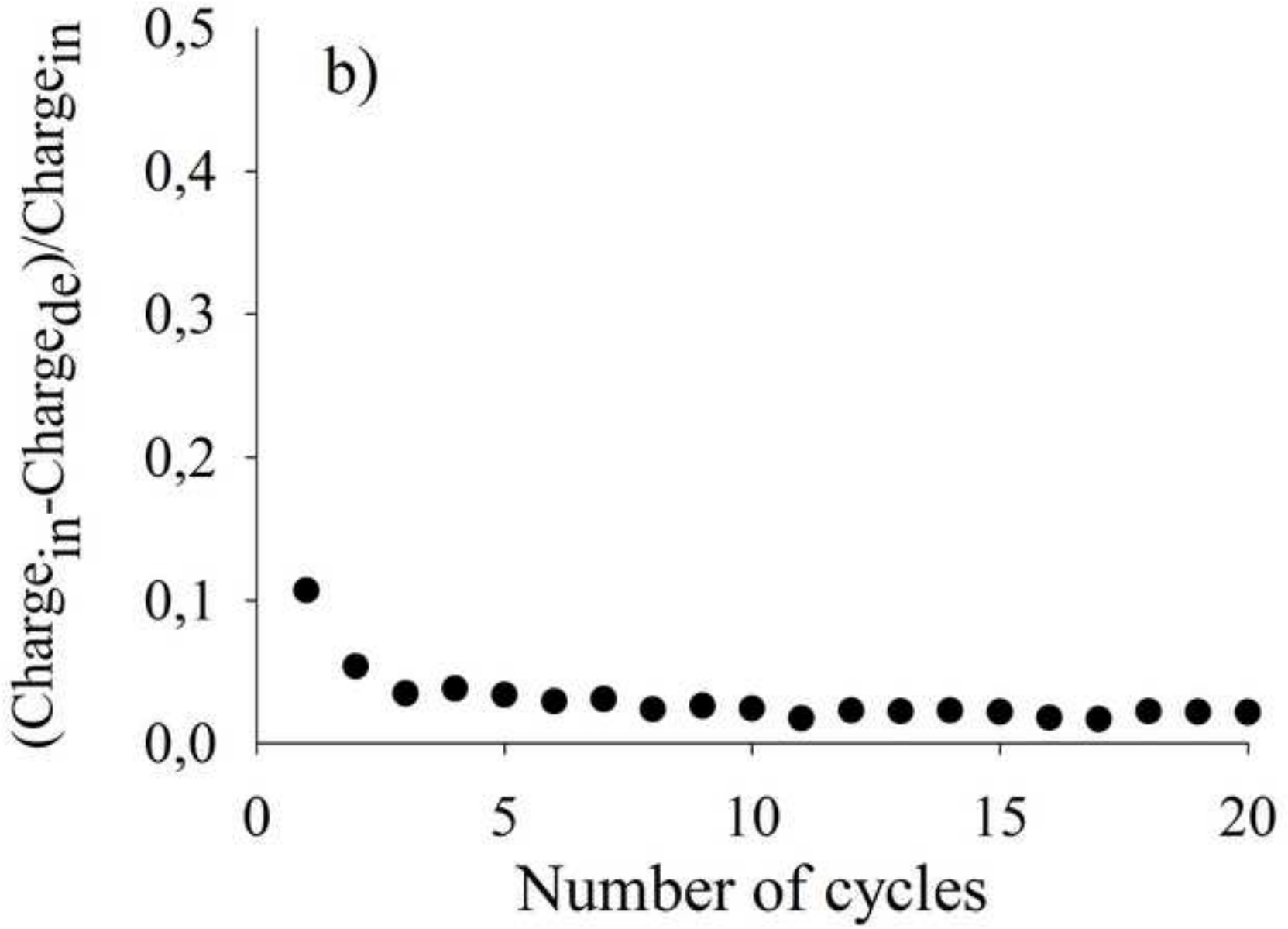
b)
(Charge$_{in}$-Charge$_{de}$)/Charge$_{in}$
0,5
0,4
0,3
0,2
0,1
0,0
0
5
10
15
20
Number of cycles

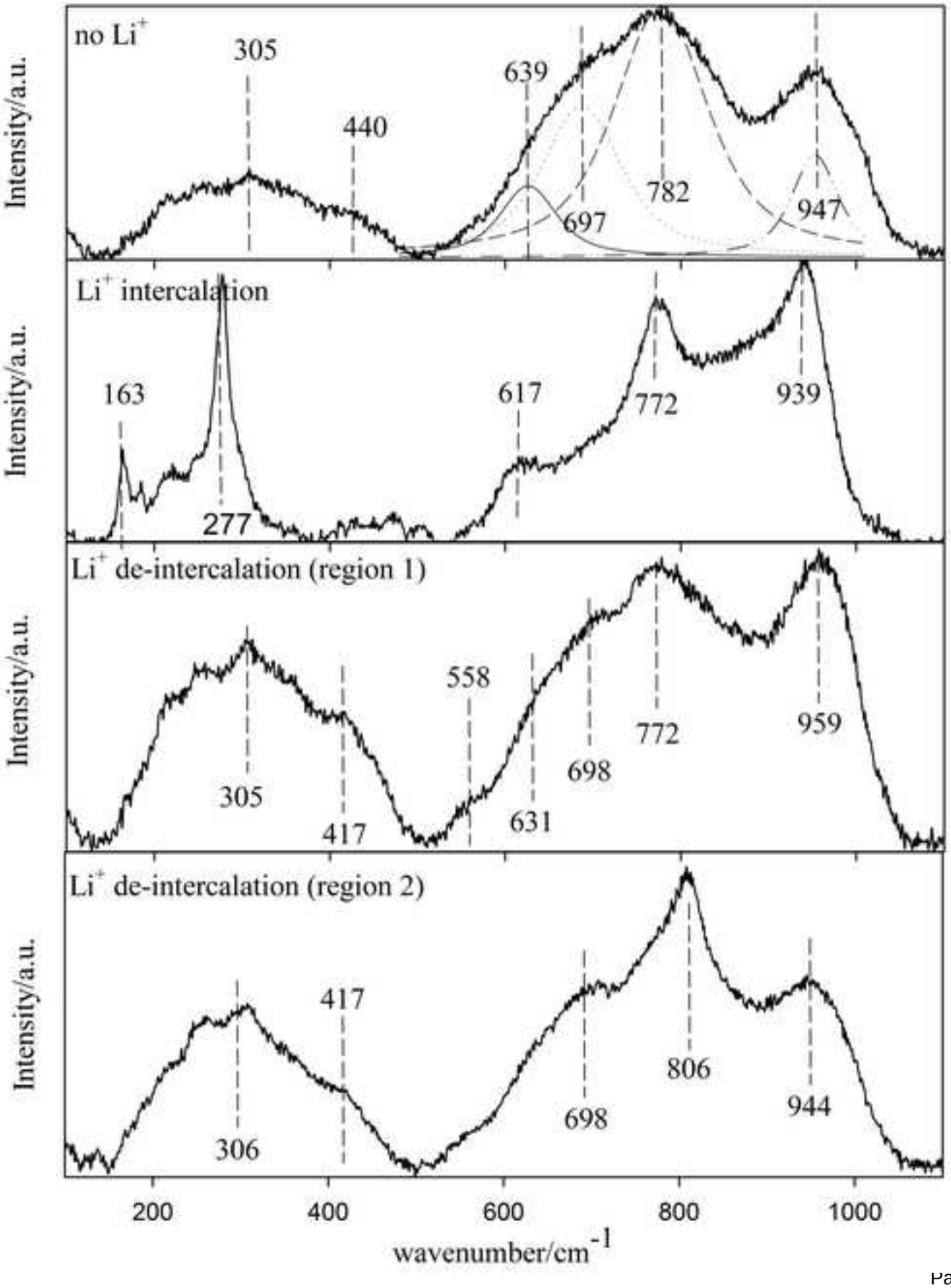

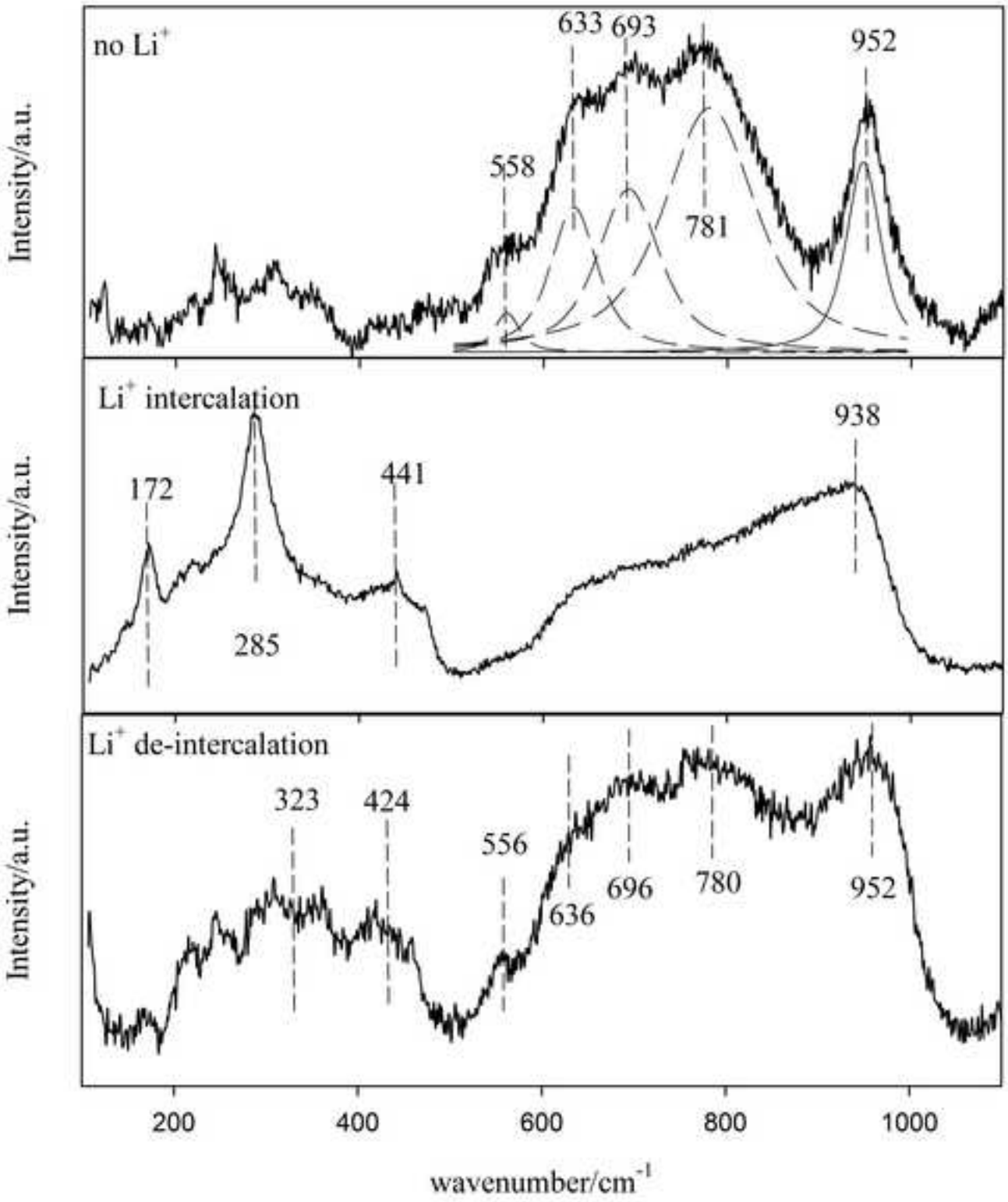

Table 1:

| Mesoporous film/$cm^{-1}$ | Dense film/$cm^{-1}$ | Peak assignment [10] |
|---|---|---|
| 644 | 663 | v-O-W-O |
| 1420 | NA* | δ-OH |
| 1642/1623 | NA* | δ-OH (structural) |
| ---- | 2345 | $CO_2$ (instrument's artifact) |
| 2568-3757 | ---- | Surface H-OH, hydroxylation and hydration |

* peaks not easily distinguishable from noise

Table 2:

| Samples | Coloration time/s $10^{th}/20^{th}$ cycles[a] | Bleaching time/s $10^{th}/20^{th}$ cycles[a] | Charge inserted/mC $cm^2$ $1^{st}/20^{th}$ cycles[a] | Charge de-inserted/mC $cm^{-2}$ $1^{st}/20^{th}$ cycles[a] | Reversibility (%) $1^{st}/20^{th}$ cycles[a] |
|---|---|---|---|---|---|
| Dense film | 48/47 | 10/10 | 42.1/27.7 | 22.4/27.4 | 53/98 |
| Mesoporous film | 24/21 | 6/5 | 35.3/24.1 | 31.5/23.6 | 89/98 |

a: Calculated from the chronoamperometric measurements

**Graphical Abstract (for review)**